Real-space Green's function approach to resonant inelastic x-ray scattering

J. J. Kas,[1] J. J. Rehr,[1,*] J. A. Soininen,[2] and P. Glatzel[3]

[1]*Department of Physics, Box 351560, University of Washington, Seattle, Washington 98195-1560, USA*

[2]*Department of Physics, P.O. Box 64, University of Helsinki, FI-00014 Helsinki, Finland*

[3]*European Synchrotron Radiation Facility, B.P. 220, F-38043 Grenoble, France*

(Received 21 January 2011; revised manuscript received 7 April 2011; published 8 June 2011)

We present an *ab initio* theory of core and valence resonant inelastic x-ray scattering (RIXS) based on a real-space multiple-scattering Green's function formalism and a quasiboson model Hamiltonian. Simplifying assumptions are made that lead to an approximation of the RIXS spectrum in terms of a convolution of an effective x-ray absorption signal with the x-ray emission cross section. Additional many-body corrections are incorporated in terms of an effective energy-dependent spectral function. Example calculations of RIXS are found to give qualitative agreement with experimental data. Our approach also yields simulations of lifetime-broadening suppressed x-ray absorption, as observed in high-energy resolution fluorescence detection experiment. Finally, possible improvements to our approach are briefly discussed.

DOI: 10.1103/PhysRevB.83.235114 PACS number(s): 78.70.Dm, 78.70.En, 78.70.Ck

I. INTRODUCTION

Resonant inelastic x-ray scattering (RIXS) is a powerful tool for probing occupied and unoccupied densities of states at high resolution. Moreover, the RIXS signal contains valuable information about the many-body excitations of a system, for example, those beyond the primary quasiparticle excitation.[1–4] However, because the RIXS signal is described by the Kramers-Heisenberg equation rather than Fermi's golden rule and is sensitive to many-body excitations, theoretical calculations of RIXS are more difficult than those of related core-level spectroscopies such as x-ray absorption (XAS), x-ray emission (XES), and electron energy loss (EELS). Even so, models of the RIXS spectrum based on single-particle band structure arguments can be quite useful for systems with weak electron correlations, that is, sp-electron systems.[5–12] To account for particle-hole interactions, methods based on the Bethe-Salpeter equation (BSE) have been employed.[13] In addition, there have been works modeling d-electron systems within the single-particle picture.[14–16] Also, for systems with strong electron correlations, the Anderson impurity model and atomic multiplet methods have been used to explain RIXS spectra of localized d- and f-state systems.[17] For more detailed reviews see, for example, Refs. 2–4.

In this paper we introduce a theoretical treatment of RIXS based on an approximation to the Kramers-Heisenberg equation that uses a real-space multiple-scattering Green's function (RSGF) formalism to describe the single-particle spectrum and a quasiboson model Hamiltonian to account for multielectron (shake-up and shake-off) excitations.[18,19] Although extensions are possible, our approach is currently limited to systems with weak correlations. Our derivation is similar in some respects to that of Ref. 12, which also uses a multiple-scattering formalism and a related treatment of inelastic losses. The main differences are that (i) our expression does not rely on a single-site approximation for the single-particle Green's function; (ii) we include quasiparticle self-energy corrections based on a many-pole model of the dielectric function; and (iii) we approximate the many-body losses via a convolution with an effective spectral function that includes intrinsic and extrinsic losses and interference effects.[19] In addition, with several simplifying assumptions, we demonstrate that the RIXS cross section can be approximated as a convolution of XAS and XES signals. This simplified formula is analogous to an approximation in terms of appropriate joint densities of states.[14,15] However, our result also explicitly includes the energy dependence of the dipole matrix elements. Other authors have also used Green's function techniques to calculate RIXS,[20] however they focused on the *indirect* RIXS spectrum in strongly correlated systems, while our formalism is meant to reproduce the *direct* RIXS and is currently limited to weakly correlated systems. To calculate our approximation to the RIXS spectrum efficiently, we have implemented the theory in an extension of the RSGF code FEFF9.[21,22] This approach has been used extensively to calculate several other core-level spectra, including XAS, XES, and EELS, as well as VIS-UV spectra.[22–25] The method has been particularly beneficial for the core-level spectra of complex systems, since it does not rely on periodic symmetry, which is generally broken by the presence of the core hole. Illustrative examples are presented that yield reasonable agreement with available experimental RIXS. Our theory also yields simulations for related spectra, for example, lifetime broadening suppressed XAS spectra, as observed in high-energy resolution fluorescence detection (HERFD) experiments.

The remainder of this article is ordered as follows. We begin by introducing the theory of RIXS starting from the Kramers-Heisenberg equation and summarizing our key results. In particular, we develop an approximate formula for the RIXS cross section in terms of a convolution of XES and effective XAS signals. We then present a more detailed derivation of RIXS in terms of quasiparticle Green's functions within the RSGF formalism. Subsequently, we present several illustrative calculations and compare with experimental data for a number of weakly correlated systems. Although our treatment is, in principle, more general, we restrict our attention in this work to systems for which the quasiparticle approximation is reasonable. Finally, we make a number of concluding remarks. Technical details are relegated to the Appendix.

II. THEORY

In RIXS experiments, x-rays are scattered off a sample, and the scattered intensity is measured as a function of the frequencies of the incident and outgoing x-rays and the momentum transfer. Qualitatively, the incident x-ray is absorbed by the system, creating a deep core hole and photoelectron along with a variety of many-body excitations, and emission occurs at a later time. At low photo-electron energies these processes are coupled and cannot be described as a two-step process. There are several "flavors" of RIXS measurements, termed *direct* and *indirect* RIXS. In direct RIXS measurements, outgoing frequencies are selected such that the scattered intensity is dominated by emission due to transitions from occupied valence (or core) levels to the deep core hole. In indirect RIXS measurements, the emitted photons are due to transitions from the excited electrons (those above the Fermi level) to the deep core hole, and thus energy losses are more directly related to secondary excitations. We do not treat the indirect RIXS here, although an extension of the present formalism to that case may be possible.

A. RIXS in terms of XAS and XES

Below we give a brief outline of the basic theory of RIXS and describe the key expressions used in our calculations. All quantities are expressed in Hartree atomic units ($e = \hbar = m = 1$) unless otherwise noted. Formally the RIXS double differential cross section is given by the Kramers-Heisenberg equation[26]

$$\frac{d^2\sigma}{d\Omega d\omega} = \frac{\omega}{\Omega}\sum_F \left| \frac{\sum_M \langle F|\Delta_2^\dagger|M\rangle\langle M|\Delta_1|\Psi_0\rangle}{E_M - \Omega - E_0 + i\Gamma_M} \right|^2 \times \delta(\Omega - \omega + E_0 - E_F). \quad (1)$$

Here Ω and ω are the energies of the incoming and outgoing photons; Δ_1 and Δ_2 are the many-body transition operators; and $|\Psi_0\rangle$, $|M\rangle$, and $|F\rangle$ are many-body electronic ground, intermediate, and final states with corresponding energies E_0, E_M, and E_F. This formula for the cross section can be expressed in terms of effective one-particle Green's functions (cf. Ref. 12 and our derivation in Sec. II C) corresponding to the intermediate and final many-body states

$$\frac{d^2\sigma}{d\Omega d\omega} = -\frac{1}{\pi}\frac{\omega}{\Omega}|\langle b|d_2 Q|c\rangle|^2 \mathrm{Im}[\langle b|d_1^\dagger P g^b(\Omega + E') \times g^c(\Omega - \omega + E_c) g^b(\Omega + E_b)^\dagger P d_1|b\rangle]. \quad (2)$$

Here the one-particle Green's functions g^b and g^c are given by

$$g^b(\omega) = \left\langle \Phi_0^b \right| \frac{1}{\omega - h_p^b - V_{pv} + i\Gamma_b} \left| \Phi_0^b \right\rangle \equiv \frac{1}{\omega - h_p^b - \Sigma_p(\omega) + i\Gamma_b},$$
$$g^c(\omega) = \frac{1}{\omega - h_p^c - \Sigma_p(\omega) + i\Gamma_c}, \quad (3)$$

where b and c denote deep and shallow core holes, $|\Phi_0^b\rangle$ is the ground state of the valence electrons in the presence of core hole b, the projection operators P and Q project onto unoccupied or occupied states of the single-particle ground-state Hamiltonian, and E_b, E_c are the core level energies. As shown in the Appendix, we can rewrite this expression in terms of a nonlocal transition operator T,

$$\frac{d^2\sigma}{d\Omega d\omega} = -\frac{1}{\pi}\frac{\omega}{\Omega}\frac{|\langle b|d_2 Q|c\rangle|^2}{|\omega + E_b - E_c + i\Gamma_b|^2} \times \mathrm{Im}[\langle b|T^\dagger(\Omega) g^c(\Omega - \omega + E_c) T(\Omega)|b\rangle], \quad (4)$$

where $T(\Omega) = [1 + \Delta V g^{b\dagger}(\Omega + E_b)] P d_1$. We now relate this result to the XES $\mu_e(\omega)$ and an XAS-like signal $\bar{\mu}(\Omega, \Omega - \omega)$:

$$\frac{d^2\sigma}{d\Omega d\omega} = \frac{\omega}{\Omega}\int d\omega_1 \frac{\mu_e(\omega_1)\bar{\mu}(\Omega, \Omega - \omega - \omega_1 + E_b)}{|\omega - \omega_1 + i\Gamma_b|^2}, \quad (5)$$

where the effective absorption coefficient $\bar{\mu}$ is

$$\bar{\mu}(\Omega, \Omega - \omega) = -\frac{1}{\pi}\mathrm{Im}[\langle b|T^\dagger(\Omega) g^c(\Omega - \omega + E_c) T(\Omega)|b\rangle]. \quad (6)$$

The quantity $\bar{\mu}$ differs from normal XAS coefficient since the dipole transition operator in XAS is replaced by $T(\Omega)$. If the matrix elements of $g^b \Delta V$ are much smaller than unity, which is the case for all but localized excitations, we may take the leading-order approximation, and thus relate the RIXS to the usual XAS coefficient $\mu(\omega)$; that is,

$$\frac{d^2\sigma}{d\Omega d\omega} \propto \frac{\omega}{\Omega}\int d\omega_1 \frac{\mu_e(\omega_1)\mu(\Omega - \omega - \omega_1 + E_b)}{|\omega - \omega_1 - i\Gamma_b|^2}. \quad (7)$$

Thus we obtain a relatively simple expression for the RIXS cross section in terms of XAS, XES, and a resonant denominator. Moreover, the terms in either expression [Eq. (5) or (7)] can be calculated within the RSGF framework using the FEFF codes.[21,22,24,27,28] It should be noted that the above expressions, Eqs. (5) and (7), are similar to those in the pioneering work of Tulkki and Åberg,[29–31] in which a derivation of electronic resonant Raman spectra is given in terms of multichannel scattering states and applied to the K_α RIXS of $KMnO_4$.

B. Multiple scattering theory

We now turn our attention to the application of the multiple-scattering RSGF formalism to Eq. (5). Within this formalism the single-particle Green's function can be expanded about the absorbing atom as[21]

$$G(\boldsymbol{r}, \boldsymbol{r}', E) = -2k\left[\sum_{LL'}|R_L(E)\rangle G_{L0,L'0}(E)\langle R_{L'}(E)| + \delta_{L,L'}|H_L(E)\rangle\langle R_L(E)|\right]. \quad (8)$$

Calculations of the RIXS cross section requires both the single-particle XES signal, which is straightforward to calculate with FEFF9, and the effective absorption cross section $\bar{\mu}$. To calculate the latter we begin by rewriting Eq. (6) in terms of the one-electron density matrix ρ^c:

$$\bar{\mu}(\Omega, \Omega - \omega) \propto \langle b|T^\dagger(\Omega)\rho^c(\Omega - \omega + E_c)T(\Omega)|b\rangle. \quad (9)$$

Note, again, that $|b\rangle$ and $|c\rangle$ signify states calculated in the presence of the deep or shallow core hole, respectively. Using

the relation $\rho = -(1/\pi)\,\mathrm{Im}\,[g]$ and inserting our expression for the Green's function, we obtain

$$\bar{\mu}(\Omega,\Omega-\omega) = -2k\sum_{LL'}\langle b|T^{\dagger}(\Omega)\big|R_L^c\rangle\big[\delta_{LL'} + \rho^c_{0L0L'}(\Omega-\omega+E_c)\big]\big\langle R_{L'}^c\big|T(\Omega)|b\rangle, \quad (10)$$

where $k=\sqrt{2(\Omega-\omega+E_c-V_{\mathrm{int}})}$ and V_{int} is the interstitial potential. In the above we have assumed that the argument $\Omega-\omega+E_c$ is real and used the result $\mathrm{Im}[|R\rangle\langle H|]=|R\rangle\langle R|$ for energies on the real axis. Note that the energy arguments of the bras and kets above have been omitted for the sake of brevity. We now turn to the matrix elements of the transition operator

$$T_{Lb}(\Omega)=\big\langle R_L^c|T(\Omega)\big|b\big\rangle=\big\langle R_L^c\big|[\Delta V g^b(\Omega)^{\dagger}+1]d_1|b\big\rangle, \quad (11)$$

where, for simplicity, we have neglected the projection operator P. Rewriting the Green's function g^b in spectral representation and, again, inserting the MS expression for the Green's function in Eq. (8) gives

$$T_{Lb}(\Omega)=\big\langle R_L^c\big|d_1|b\big\rangle+\pi\int d\omega_1\frac{2k_1}{\omega_1+i\Gamma_b}\sum_{L_1}\big\langle R_L^c\big|\Delta V\big|R_L^b\big\rangle \times\big[\delta_{LL_1}+\rho^b_{LL_1}(\Omega-\omega_1)\big]\big\langle R^b_{L_1}\big|d_1|b\big\rangle, \quad (12)$$

where, again, $k_1=\sqrt{2(\Omega-\omega_1-V_{\mathrm{int}})}$. Thus in addition to the usual dipole matrix elements, we have a second term that depends on both energies in the problem: the incoming photon frequency Ω and the energy loss $\Omega-\omega$.

C. Many-body effects and the quasiboson model

In this subsection we discuss the application of the quasiboson model to calculations of inelastic loss effects in RIXS. We begin here by rewriting Eq. (1) in terms of the many-body Green's functions. To do this, we express the RIXS amplitude as

$$\tau_F(\Omega)=\sum_M\langle F|\Delta_2^{\dagger}\frac{|M\rangle\langle M|}{\Omega+E_0-E_M-i\delta}\Delta_1|\Psi_0\rangle \quad (13)$$

$$=\langle F|\Delta_2^{\dagger}G(E)^{\dagger}\Delta_1|\Psi_0\rangle. \quad (14)$$

Inserting this last expression into Eq. (1) and using a spectral representation of the many-body density operator,

$$\rho(E)=-\frac{1}{\pi}\mathrm{Im}[G(E)]=\sum_F|F\rangle\langle F|\delta(E-E_F), \quad (15)$$

we obtain

$$\frac{d^2\sigma}{d\Omega d\omega}=\frac{\omega}{\Omega}\langle\Psi_0|\Delta_1^{\dagger}G(\xi_1)\Delta_2\rho(\xi_2)\Delta_2^{\dagger}G(\xi_1)^{\dagger}\Delta_1|\Psi_0\rangle, \quad (16)$$

where $\xi_1=\Omega+E_0$ and $\xi_2=\Omega+E_0-\omega$. Assuming that the absorption occurs from a deep core level $|b\rangle$ and employing the dipole approximation for the transition operators in Eq. (1) gives

$$\Delta_1=\sum_k\langle k|d_1|b\rangle c_k^{\dagger}b+\mathrm{h.c.},$$
$$\Delta_2=\sum_k\langle b|d_2|k\rangle b^{\dagger}c_k+\mathrm{h.c.} \quad (17)$$

If we neglect exchange terms between the particle and the hole, or at least assume that they are dealt with via an effective single-particle potential, we can write the many-body ground state as

$$|\Psi_0\rangle=|\Phi_0\rangle|b\rangle|k_2\rangle, \quad (18)$$

where k_2 is associated with a specific term in the sum over states in Δ_2, $|b\rangle$ is the deep core state excited by the absorption event, and $|\Phi_0\rangle$ is an $N-2$ electron wave function. Note that this approximation is only justified if k_2 denotes a core electron or a high-energy photoelectron, although we use the approximation for valence electrons as well. This gives

$$\Delta_1^{k_1}|\Psi_0\rangle=M_1^{k_1b}|\Phi_0\rangle|k_2\rangle|k_1\rangle\theta\big(E_{k_1}-E_{\mathrm{F}}\big),$$
$$\Delta_2^{k_2}|\Phi_0\rangle|k_2\rangle|k_1\rangle=M_2^{bk_2}|\Phi_0\rangle|b\rangle|k_1\rangle\theta\big(E_{\mathrm{F}}-E_{k_2}\big), \quad (19)$$

where $M_i^{kb}=\langle k|d_i|b\rangle$ and

$$H|\Psi_0\rangle=E_0|\Psi_0\rangle=\big(\epsilon_b+\epsilon_{k_2}+E_0^0\big)|\Psi_0\rangle. \quad (20)$$

Here E_{F} is the Fermi energy. Then the RIXS cross section becomes

$$\frac{d^2\sigma}{d\Omega d\omega}=-\frac{1}{\pi}\frac{\omega}{\Omega}\mathrm{Im}\left[\sum_{k_1k_2}^{\mathrm{unocc}}\sum_{k_3k_4}^{\mathrm{occ}}M_2^{bk_3}\big(M_2^{k_4b}M_1^{bk_1}\big)^*M_1^{k_2b} \times\langle k_1|\langle k_3|\langle\Phi_0|K_{k_3k_4}(\xi_1,\xi_2)\,|\Phi_0\rangle|k_4\rangle|k_2\rangle\right], \quad (21)$$

where K is given by

$$K_{kk'}(\omega,\omega')=G(\omega)c_k^{\dagger}bG(\omega')b^{\dagger}c_{k'}G(\omega)^{\dagger}, \quad (22)$$

and $G(E)=1/(E-H+i\delta)$ is the many-body Green's function. We now introduce a quasiboson approximation to the Hamiltonian following the treatment in Ref. 18. In this approach the excitations of the many-body valence electronic states are represented as bosons, while the photoelectron and hole are treated via an effective single-particle theory,

$$H=H_0^{N-2}+h_p+h_h+V_{hv}+V_{pv}+V_{ph}, \quad (23)$$

where h_h and h_p are the one-particle Hamiltonians for the hole and particle, respectively, V_{hv}/V_{pv} describes the interaction of the hole/particle with the valence electrons,

$$h_p=\sum_k\epsilon_kc_k^{\dagger}c_k,\quad h_h=-\sum_k\epsilon_kc_kc_k^{\dagger}, \quad (24)$$

$$V_{pv}=\sum_{n,k_1k_2}\big[V^n_{k_1k_2}a_n^{\dagger}+\big(V^n_{k_1k_2}\big)^*a_n\big]c_{k_1}^{\dagger}c_{k_2}, \quad (25)$$

$$V_{hv}=\sum_{n,k_1k_2}\big[V^n_{k_1k_2}a_n^{\dagger}+\big(V^n_{k_1k_2}\big)^*a_n\big]c_{k_1}c_{k_2}^{\dagger}, \quad (26)$$

and V_{ph} describes the interaction between the photoelectron and the hole. This last interaction should in principle be treated via the BSE; however, here we approximate it either by using a self-consistent final-state rule approximation for deep core holes (i.e., with the screened core-hole potential of the deep core hole), or by neglecting it altogether, as in the initial state rule (independent particle approximation) for valence holes. Experience with such models using the FEFF code shows that these approximations are reasonable for many

systems. The bosons in the above approximation correspond to neutral excitations. Depending on the coupling constants, they can represent plasmons, particle-hole states, phonons, or other such excitations and could, in principle, even be used to represent strongly localized excitations.[18,19,32–34] In this work, however, we have limited our investigation to plasmonic and particle-hole excitations.

We now define $|\Phi_0^b\rangle$ as the ground state of the $N-2$ electron system in the presence of the deep core hole $|b\rangle$, and $|\Phi_0^c\rangle$ as the ground state of the $N-2$ electron system in the presence of the second core hole $|c\rangle$ so that

$$\begin{aligned} H^b\big|\Phi_0^b\big\rangle &= E_0^b\big|\Phi_0^b\big\rangle; \quad H^b = H_0^{N-2} + V_{hv}^b, \\ H^c\big|\Phi_0^c\big\rangle &= E_0^c\big|\Phi_0^c\big\rangle; \quad H^c = H_0^{N-2} + V_{hv}^c, \end{aligned} \tag{27}$$

with core level energies

$$\begin{aligned} E_b &= \epsilon_b - E_0^0 + E_0^b, \\ E_c &= \epsilon_c - E_0^0 + E_0^c. \end{aligned} \tag{28}$$

The transition matrix elements corresponding to emission (d_2) may be pulled outside the imaginary part, and serve as an amplitude factor, that is,

$$\begin{aligned} \frac{d^2\sigma}{d\Omega d\omega} = -\frac{1}{\pi}\frac{\omega}{\Omega}\sum_c |\langle b|d_2 Q|c\rangle|^2 \\ \times \mathrm{Im}\left[\sum_{k_1k_2}^{\mathrm{unocc}} \langle b|d_1^\dagger P\langle\Phi_0|F(E_1,E_2)|\Phi_0\rangle P d_1|b\rangle\right]. \end{aligned} \tag{29}$$

Here $E_1 = \Omega + E_b$, $E_2 = \Omega + E_c - \omega$, P is a projector onto unoccupied states of the ground-state Hamiltonian, Q is a projector onto occupied states of the intermediate-state Hamiltonian,

$$F(E_1,E_2) = G^b(E_1)G^c(E_2)G^{b\dagger}(E_1), \tag{30}$$

and finally, the Green's functions are calculated in the presence of the deep (b) or shallow (c) core hole, that is,

$$\begin{aligned} G^b(\omega) &= \frac{1}{\omega - \left(H^b - E_0^b\right) - h_p^b - V_{pv} + i\Gamma_b}, \\ G^c(\omega) &= \frac{1}{\omega - \left(H^c - E_0^c\right) - h_p^c - V_{pv} + i\Gamma_c}. \end{aligned} \tag{31}$$

Next we derive an expression for the effects of multielectron excitations in terms of an effective spectral function. Within the quasiboson approximation, the following relationships among the eigenstates of H_0, H_0^b, and H_0^c hold:[18,19]

$$\begin{aligned} |\Phi_0\rangle &= e^{-S_b}\big|\Phi_0^b\big\rangle; \quad S_b = \frac{a_b}{2} - \sum_n \frac{V_{bb}^n}{\omega_n} a_{bn}^\dagger, \\ \big|\Phi_0^b\big\rangle &= e^{-\Delta S}\big|\Phi_0^c\big\rangle; \quad \Delta S = \frac{\Delta a}{2} - \sum_n \frac{\Delta V^n}{\omega_n} a_{cn}^\dagger, \\ \Delta a &= \sum_n \left(\frac{\Delta V^n}{\omega_n}\right)^2, \quad a_b = \sum_n \left(\frac{V_{bb}^n}{\omega_n}\right)^2. \end{aligned} \tag{32}$$

Here $\Delta V^n = V_{cc}^n - V_{bb}^n$ is the difference between the intermediate- and the final-state core-hole potentials. If we assume only single-boson excitations, we can also write

$$\big|\Phi_n^b\big\rangle = \left[a_{cn}^\dagger - \frac{\Delta V^n}{\omega_n}\right] e^{-\Delta S}\big|\Phi_0^c\big\rangle, \tag{33}$$

which will give us the correct expression to second order in the couplings when used in our formula for the RIXS signal. Ignoring the off-diagonal terms in V_{pv} we obtain

$$\begin{aligned} \langle\Phi_0|F(E_1,E_2)|\Phi_0\rangle = \Bigg\{\sum_{n_1n_2} \big\langle\Phi_0^b\big|e^{-S_b{}^\dagger} G^b(E_1)\big|\Phi_{n_1}^b\big\rangle\big\langle\Phi_0^c\big|e^{-\Delta S^\dagger} \\ \times \left[a_{cn_1} - \left(\frac{\Delta V^{n_1}}{\omega_{n_1}}\right)^*\right] G^c(E_2) \\ \times \left[a_{cn_2}^\dagger - \frac{\Delta V^{n_2}}{\omega_{n_2}}\right] e^{-\Delta S}\big|\Phi_0^c\big\rangle\big\langle\Phi_{n_2}^b\big| \\ \times [G^b(\Omega + E_c)]^\dagger e^{-S_b}\big|\Phi_0^b\big\rangle\Bigg\}. \end{aligned} \tag{34}$$

Note that in the case of valence emission (valence hole), we are assuming that the core-hole potential is negligible, hence $E_c = \epsilon_c$, and $\Gamma_c = 0$. We now define the amplitudes to create a single boson as

$$\alpha_n^b = V^n G^b(E_1) - \frac{V_{bb}^n}{\omega_n}, \quad \alpha_n^c = V^n G^c(E_2) - \frac{\Delta V^n}{\omega_n}, \tag{35}$$

and the amplitudes to annihilate a boson as

$$\beta_n^b = G^b(E_1)(V^n)^* - \frac{V_{bb}^n}{\omega_n}, \quad \beta_n^c = G^c(E_2)(V^n)^* - \frac{\Delta V^n}{\omega_n}. \tag{36}$$

Expanding to second order in the amplitudes to create and annihilate bosons and neglecting of-resonant terms, that is, those that contain a G^b, $G^{b\dagger}$ with different energy arguments, gives two terms quadratic in the coupling constant plus the zeroth-order term,

$$\begin{aligned} \langle\Phi_0|F(E_1,E_2)|\Phi_0\rangle = e^{-a^c}\big\{G_0^b(E_1)G_0^c(E_2)G_0^{b\dagger}(E_1) \\ + G_0^b(E_1)\beta_n^c G_n^c(E_2)\alpha_n^c G_0^{b\dagger}(E_1) \\ + \beta_n^b G_n^b(E_1)G_n^c(E_2)\big[\beta_n^b G_n^b(E_1)\big]^\dagger\big\}, \end{aligned} \tag{37}$$

where we have used the shorthand notation $G_n^b(E) = \langle\Phi_0^b|G^b(E-\omega_n)|\Phi_0^b\rangle$, and similarly for $G_n^c(E)$. The total cross section may now be written in terms of a convolution of the single-particle cross section $\left[d^2\sigma/d\Omega d\omega\right]_{\mathrm{sp}}$, as given in Eq. (5), with an effective spectral function A_{eff},

$$\begin{aligned} \frac{d^2\sigma}{d\Omega d\omega} = \int d\omega_1 d\omega_2\, A_{\mathrm{eff}}(\Omega,\Omega-\omega,\omega_1,\omega_2) \\ \times \left[\frac{d^2\sigma}{d\Omega d\omega}\right]_{\mathrm{sp}}\Bigg|_{\Omega=\Omega-\omega_1,\omega=\omega-\omega_1+\omega_2}, \end{aligned} \tag{38}$$

where the spectral function is given by

$$\begin{aligned} A_{\mathrm{eff}}(E_1,E_2,\omega_1,\omega_2) = e^{-a_c}\{\delta(\omega_1)\delta(\omega_2) \\ + \sum_n [\beta_{cn}(E_2)\alpha_{cn}(E_2)\delta(\omega_1)\delta(\omega_2-\omega_n) \\ + |\beta_{bn}(E_1)|^2\delta(\omega_1-\omega_n)\delta(\omega_2-\omega_n)]\}. \end{aligned} \tag{39}$$

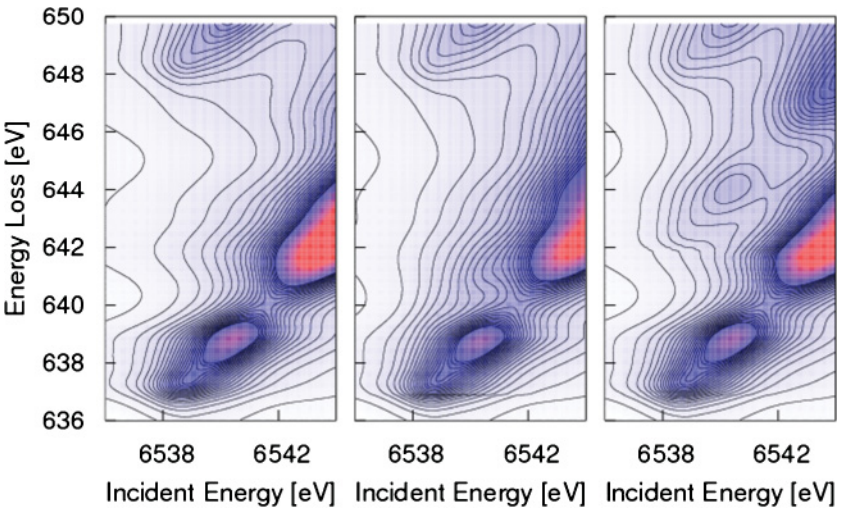

FIG. 1. (Color online) Mn K_α RIXS of MnO calculated with a plasmon pole spectral function with varying plasmon frequencies. Quasiparticle only (left) is compared to convolutions, $\omega_p =$ 2 eV (middle) and $\omega_p = 5$ eV (right).

Note that because the total excitation amplitudes α_n and β_n include both extrinsic and intrinsic amplitudes, the above expression also includes interference terms. These interference terms tend to cancel the intrinsic and extrinsic satellites, and at least for XAS in metals, this cancellation becomes near complete close to threshold.[18] It should be noted that our current formalism for the spectral function is not directly suited for highly correlated materials, although an extension of the quasiboson model Hamiltonian to such cases may be possible.[32,33] The application of the spectral function to RIXS is similar to that in Refs. 18 and 19, where a convolution was applied to XAS. The approximations made in the above references for obtaining the quasiboson excitations were based on plasmon-like dispersion. Plasmon satellites are expected to contribute to the spectrum only at frequencies (relative to threshold) higher than the plasma frequency, which is typically about 10–20 eV. For the results shown in this paper, the main plasmon excitation satellites are outside the range of experimental data. In addition, the interference terms tend to diminish the effects of the intrinsic and extrinsic satellites. There can, however, be strong localized excitations near threshold, for example, charge transfer excitations or dd^* excitations. It may be possible to represent these via a quasiboson model as well, but this is beyond the scope of this paper. In Fig. 1 we show the effect of a single plasmon pole model spectral function on the spectrum for several plasma frequencies. We have set the weight of the satellite to 0.3, which is probably larger than expected for plasmonic excitations but gives us an idea of the possible effects of more localized excitations.

For the results presented in Sec. IV we restrict our calculations to the quasiparticle approximation, that is, with the spectral function replaced by a δ function,

$$A_{\text{eff}}(E_1,E_2,\omega_1,\omega_2) = \delta(\omega_1)\delta(\omega_2 - \omega_n), \tag{40}$$

which amounts to neglecting satellite peaks due to multielectron excitations. The use of this approximation causes the calculated spectral lineshapes to be more symmetric than experimental results, since the main quasiparticle peak is modeled in Eq. (40) as a Lorentzian. In general multielectron excitations lead to asymmetric peaks, so that Eq. (39) has a Fano-type main lineshape.

III. EXPERIMENT

The experimental results presented in this paper are the product of work performed at beamline ID26 of the European Synchrotron Radiation Facility (ESRF). Below we describe the experimental procedures and techniques. The incident energy was selected by means of a pair of cryogenically cooled Si crystals in (311) reflection with an energy bandwidth of 0.2 eV (0.3 eV) at 4.9 keV (6.5 keV). The incident flux on the sample was 1×10^{13} photons/s using the fundamental peak of the undulator radiation. The beam size on the sample was 0.2 mm vertical by 1.0 mm horizontal. Higher harmonics were suppressed by three Si mirrors operating in total reflection. The resonantly scattered x-rays were analyzed using the (331) and (400) reflection of spherically bent Ge single-crystal wafers for the Ti K_β and K_α emission, respectively. The Ge (333) reflection was used for Mn K_α. Sample, analyzer crystals and an avalanche photodiode were arranged in a vertical Rowland geometry ($R = 1$ m) at a $90 \pm 3^\circ$ scattering angle. The combined instrumental energy bandwidth was 0.8–1.0 eV. All samples were purchased from Aldrich and used as is. Self-absorption effects distort the spectral shape and let the K absorption pre-edge region appear stronger relative to the edge jump. These effects are negligible in the K absorption pre-edge region and the samples were not diluted for the measurements.

IV. RESULTS AND DISCUSSION

A. RIXS

Calculations of RIXS were carried out for several materials based on the present theoretical approach using an extension of the RSGF code FEFF9 applied to Eq. (38). All results were calculated using self-consistent potentials and a full multiple scattering (FMS) treatment of the Green's functions for suitably large clusters centered at the core absorption site. The core-hole screening was calculated using the random phase approximation,[36] and nonspherical parts of the core-hole potential were neglected. Self-energy effects are approximated using the many-pole model self-energy[19] applied as a convolution of the single-particle spectrum, as detailed in Ref. 37. This self-energy includes both real and imaginary parts, which account, respectively, for quasiparticle phase

shifts and damping of the spectrum. These self-energy effects are rather small for low excitation energies, and thus the RIXS comparisons at low energies are not significantly affected by the quasiparticle contribution to the self-energy. At higher energies, however, such as those seen in the HERFD XAS calculations, the effects on the spectra are quite noticeable. To simplify the calculations, the Green's functions are restricted to include only the site and angular momentum diagonal elements. We find that for the cases presented here, the angular momentum diagonal approximation is reasonable for all but the lowest energy peaks since the overlap with ΔV is then small, and our approximation becomes equivalent to Eq. (7) in terms of XES and XAS, where the angular momentum diagonal elements dominate due to dipole selection rules. To obtain a better agreement with the the experimental threshold energy, we allowed a small shift of the calculated Fermi energy, which is typically too high by about 1 eV, in the self-consistent FEFF9.0 calculation. In addition, overall energy shifts were added in each axis to align the calculation with the energy scale in the experiment. In the case of K_α RIXS, atomic values were used for the splitting between the $P_{1/2}$ and the $P_{3/2}$ emission energies.[38] In addition, the amplitudes were taken from simple counting arguments to have a ratio $A_{3/2}/A_{1/2} = 2$; however, this ratio is not generally accurate, since the particle-hole interaction mixes the hole states. Figure 2 presents a comparison of our calculated (right) Mn K_α RIXS of MnO and experiment (left). The overall agreement is qualitatively satisfactory: all main features of the experiment are reproduced including both the dipole and the quadrupole pre-edge peaks. The main edge is also at about the correct energy, although the asymmetry caused by multielectron excitations is absent in our calculation which is restricted to the quasiparticle level, where the spectral function is given by Eq. (40). We expect that going beyond this quasiparticle approximation for the spectral function as in Eq. (39) would capture some of the asymmetry since the Lorentzian spectral shape currently used for the quasiparticle peak in these calculations would be replaced by

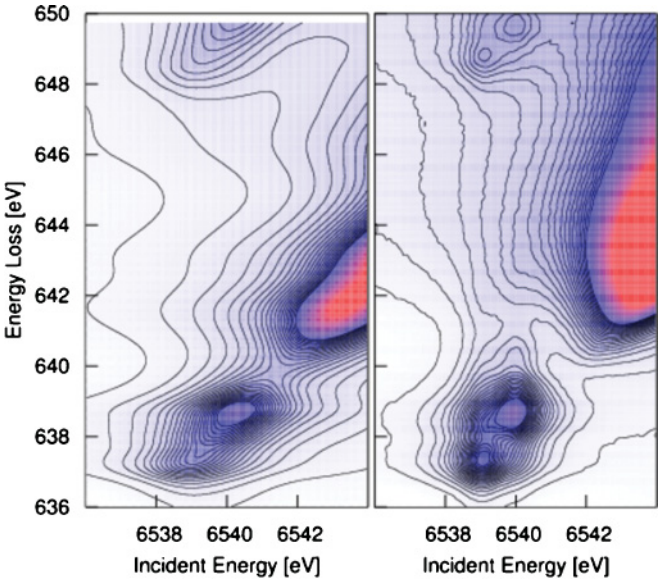

FIG. 2. (Color online) Calculated (left) Mn K_α RIXS of MnO based on Eq. (38) compared to experiment (right).[35]

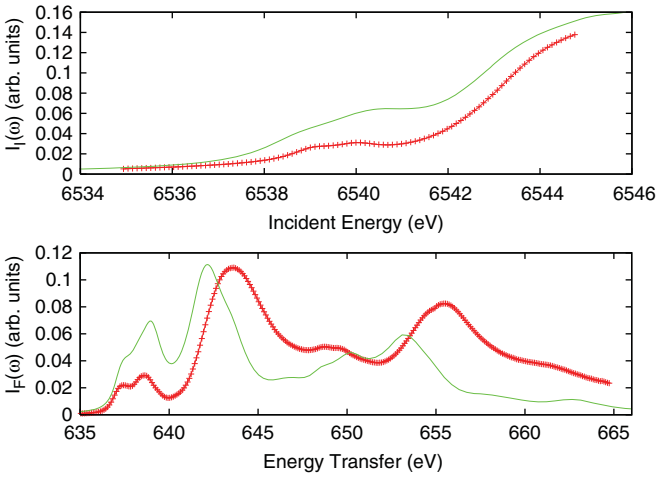

FIG. 3. (Color online) Intensity of the RIXS signal integrated over the transferred (top) and incident (bottom) energy axes. Theoretical results (solid) are compared to experiment (crosses).

a Fanotype lineshape. In addition, new features may arise due to satellite peaks in the spectral function. The main diagonal structure in our calculation appears to be sharper than that of the experiment, possibly due to self-absorption effects in the experimental data. Note that the pre-edge peak for this case is essentially on the diagonal; that is, the emission energy is the same for the pre-edge peak as for the main edge. Figure 3 shows the RIXS spectrum integrated over the transferred (top) and incident (bottom) energies. Again, we see that the theoretical results are in good qualitative agreement with experiment. The incident energy spectrum (top) is relatively featureless, although the few peaks appearing in the experiment are reproduced by the calculation. The energy transfer spectrum (bottom) has much more structure, part of which is due to the emission lines from $p_{3/2}$ and $p_{1/2}$ states. This causes the first three peaks to be replicated starting at ≈650 eV. The ratio of the $p_{3/2}$-to-$p_{1/2}$ signal is larger in the calculation; however, this is due to mixing of the core-hole states by the interaction with the photoelectron, which is not taken into account in the calculations. One way of calculating this mixing is to use either time-dependent density-functional theory (TDDFT) or a BSE treatment of the final-state core hole. In addition, the calculated amplitude of the pre-edge peaks at ≈637 eV is too large. This may be due either to the muffin-tin approximation or to spin interactions between the photoelectron and the valence, which were also neglected in our calculations.

Core-hole effects are important for a variety of excited-state spectroscopies, including EELS and XAS as well as RIXS.[1,39] RIXS spectra, in particular, however, can give us insight into these effects since the intermediate and final states have different core holes and lifetimes.[40] To illustrate the effect of different final-state core holes, we calculated the RIXS for Ti K_α, K_β, and $K_{valence}$ RIXS of TiO_2 Anatase. To obtain reasonable results for the quadrupole peak in the K-edge absorption, we increased the strength of the core-hole potential by using a 95% screened core hole and 5% bare core hole, and kept the same ratio for all core-hole calculations. Note that our calculation again reproduces all peaks, although the intensity of the calculated quadrupole peaks is weak compared to that observed in the experiment for these cases. There is

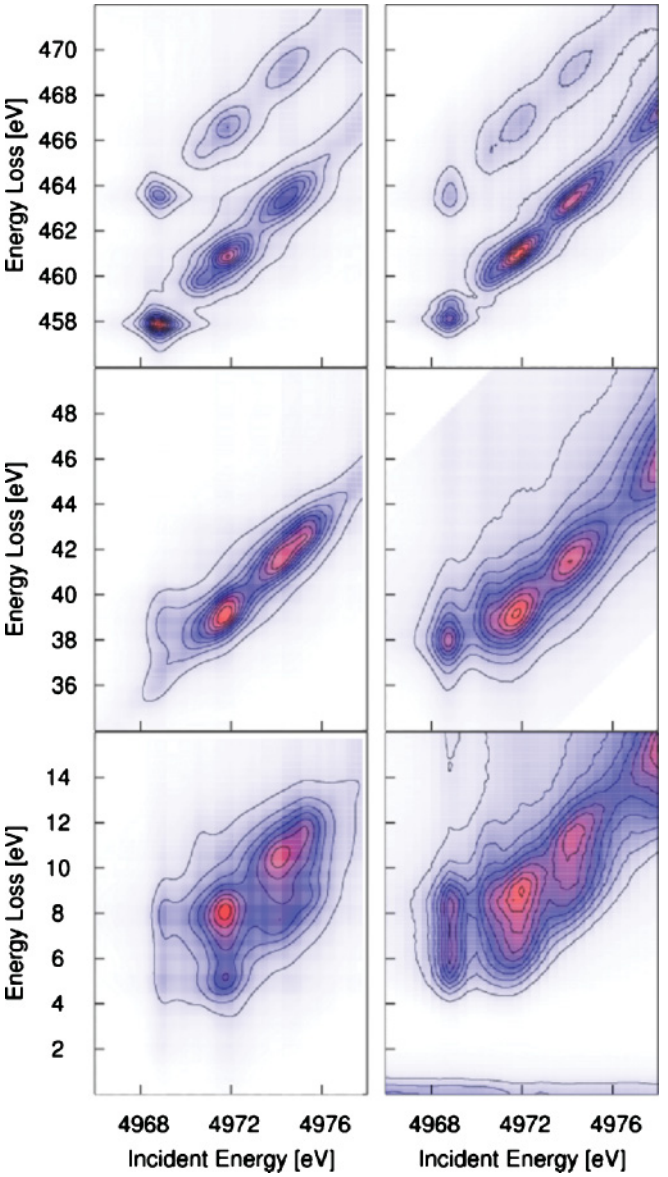

FIG. 4. (Color online) Calculated RIXS (left) of TiO_2 based on Eq. (38) compared to experiment (right) for (top to bottom) Ti K_α, K_β, and K_{valence} RIXS.

also a noticeable effect on the spectrum due to changes in the final-state core hole. For the K_α RIXS, the intermediate (1s) and final (2p) core holes are both quite localized and the difference ΔV is small, thus peaks should occur roughly on the diagonal, as shown by Eq. (12). For the K_β spectrum the final state has a 3p core hole, and the core-hole potential has a shape vastly different from that of the 1*s* core-hole potential. This causes ΔV to be large, and we expect off-diagonal peaks to be present. This is indeed the case, although only the quadrupole peaks are off-diagonal. This is due to the fact that the dipole pre-edge peaks are caused by *p*-*d* hybridization between the absorbing atom and the neighboring Ti atoms and, thus, are relatively unaffected by the core-hole potential. The quadrupole peaks, however, are due to a direct transition to the Ti *d* states, which are localized around the absorbing atom and are affected by the core-hole potential to a greater extent than the hybridized *p* states. The effect is also present

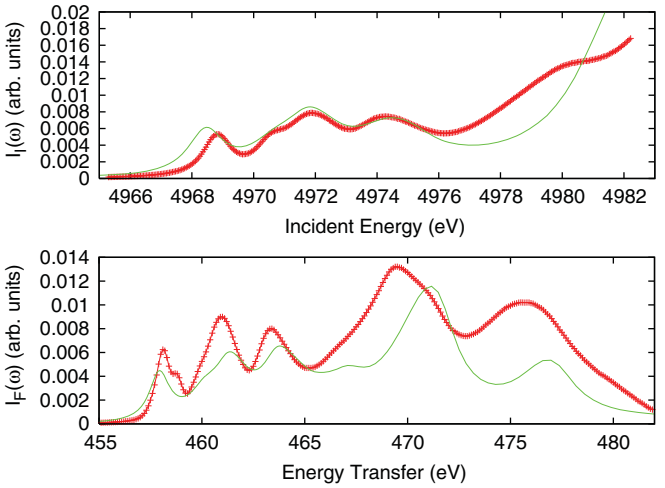

FIG. 5. (Color online) Intensity of the Ti K_α RIXS signal of TiO_2 integrated over the transferred (top) and incident (bottom) axes. Theoretical results (solid) are compared to experiment (crosses).

in the valence spectrum. In addition, the valence spectrum has multiple peaks due to the fact that the emission is from a broad valence band that is split by solid-state effects. The qualitative structure of the valence band is also well described by the calculation and reproduces the double-peak structure with the correct splitting. The intensities are also qualitatively correct, with the lower energy-transfer peaks being less intense than the higher energy-transfer peaks. The gap is too small in our calculation, however, this could be corrected via a GW gap correction. Note that we have not included the elastic scattering contribution in our calculation of the valence RIXS, which could effect the overall asymmetry of the signal. Finally, for all three spectra, the main edge occurs at a higher energy in the calculated results than in the experiment. This could be due to strong correlation effects, which are expected to shift the Ti *d* states closer to the *p* states. Another possible explanation is the inaccuracy of the spherical muffin-tin approximation,[39] which is significant in the case of Ti K pre-edge XAS of rutile TiO_2.

Figures 5–7 show the integrated intensities of Ti K_α, K_β, and K_{valence} RIXS spectra, similar to those in Fig. 4. While

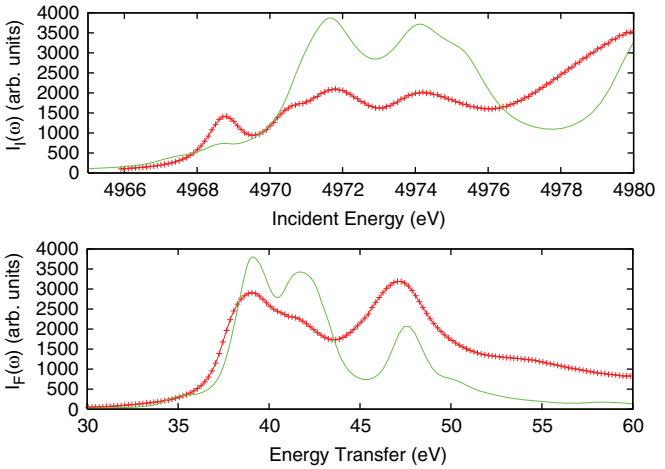

FIG. 6. (Color online) Intensity of the Ti K_β RIXS signal of TiO_2 integrated over the transferred (top) and incident (bottom) axes. Theoretical results (solid line) are compared to experiment (crosses).

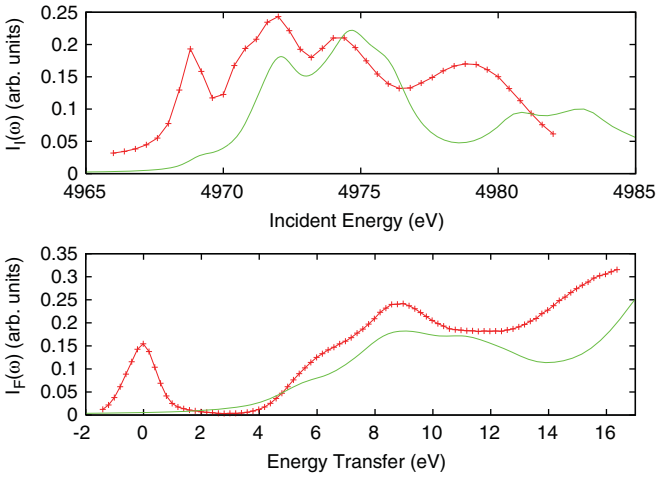

FIG. 7. (Color online) Intensity of the Ti $K_{valence}$ RIXS signal of TiO_2 integrated over the transferred (top) and incident (bottom) axes. Theoretical results (solid line) are compared to experiment (crosses). Note that the peak in experiment at zero energy transfer is the elastic peak, which was not modeled in the calculation.

the agreement between theory and experiment is quite good for the K_α spectra, the agreement in the other two cases is somewhat less satisfactory. This could be due to the neglect of the site and angular momentum off-diagonal elements of the Green's functions, which affect the pre-edge peaks more than those at higher energies, and would be more apparent in cases where the difference in intermediate- and final-state core-hole potentials ΔV is large.

B. Lifetime broadening suppressed XAS

In addition to the RIXS planes, there are several methods for obtaining lifetime broadening suppressed LBS XAS. In HERFD XAS,[41] an approximate absorption spectrum is found by the partial fluorescence yield, using a detector with a resolution higher than the natural width due to core-hole lifetime effects. This corresponds to viewing the spectra of constant emission energy in the RIXS plane. Another method of obtaining lifetime broadening suppressed XAS is to set the

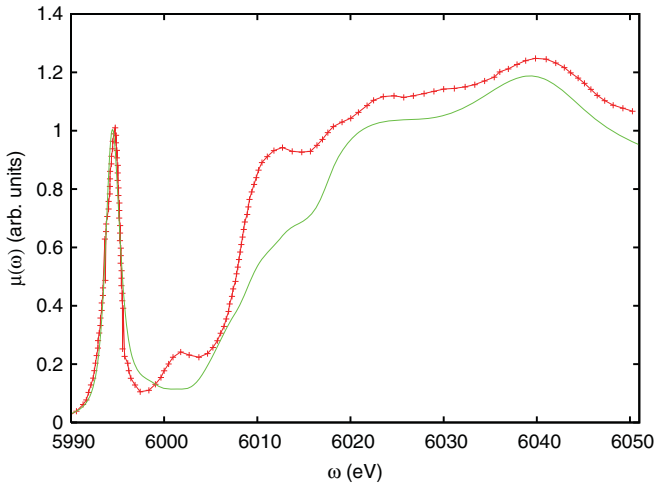

FIG. 8. (Color online) Experimental (crosses) Cr K-edge HERFD XAS[43] of K_2CrO_4 compared to our calculated results (solid line).

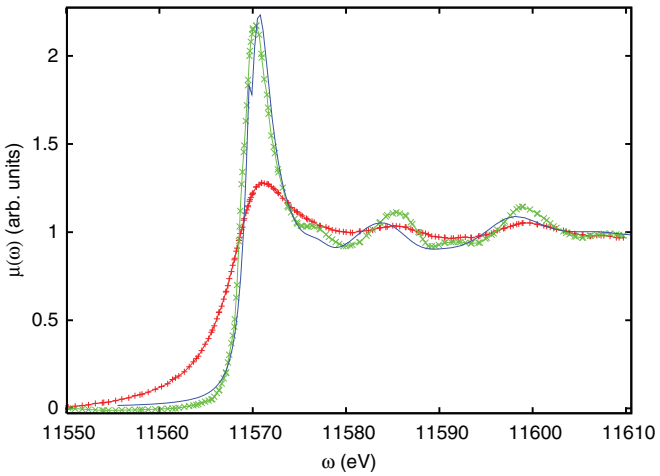

FIG. 9. (Color online) Pt L_3 edge normal XANES (crosses) compared with HERFD XAS (exes) and our calculated result (solid line).

incident energy at a point well below the edge while scanning the emission energy.[42] Under certain assumptions, the spectrum obtained in this way is approximately proportional to the XAS signal multiplied by a Lorentzian with the width of the intermediate-state core hole. For both of our calculations, we have aligned the edge with the experimental result. In Fig. 8 we show a comparison of experimental Cr-K edge HERFD XAS of K_2CrO_4 with our calculated results. We find reasonable qualitative agreement, with the exception of the peak just above 6000 eV, which is not seen in the calculation. We note, however, that the size of this peak is sensitive to distortions. In addition, the amplitude of the main peak after the rising edge is too small. This could be due to the approximate treatment of the core-hole interaction or corrections to the spherical muffin-tin potentials used in FEFF9. Figure 9 shows a comparison of bulk metallic Pt L_3 edge XANES compared to HERFD XAS and our calculated results. For this case all of the features are well reproduced, although the broadening is too large at high energies, and the higher energy peaks are also red-shifted toward the edge in comparison to the experimental result. This could be a failure of our model self-energy to accurately treat the interaction with the localized d states.[44]

V. CONCLUSIONS

We have presented a theory of RIXS that is amenable to practical calculations. Starting from the Kramers-Heisenberg equation, we derive an expression for the RIXS cross section that can be calculated within the RSGF formalism as an extension of current XAS and XES codes. Inelastic losses and quasiparticle effects are included in terms of an effective spectral function that is obtained from a quasiboson model Hamiltonian. These many-body effects are incorporated into a single-particle approximation via a convolution with an effective spectral function. Quasiparticle self-energy effects are included based on a many-pole model of the dielectric function. Approximating the many-body states as a product of an $N-2$ electron state with either two core electronic states (i.e. the ground state) or a core and photoelectron state (intermediate and final states) gives the cross section

in terms of effective single-particle Green's functions. The additional approximation that the intermediate and final photoelectron states are orthogonal with identical energies (valid at high photoelectron energies) gives the signal in terms of a convolution of the XAS and XES spectra. In addition, we have derived a formulation of the core-core RIXS spectrum that, due to the localized nature of ΔV, depends primarily on the Green's functions evaluated close to the absorbing atom. The extent of this localization is yet to be investigated, although the degree of agreement between our calculations and experimental data suggests that the on-site approximation is valid for the systems illustrated here. In addition, the on-site approximation provides a good qualitative agreement for the core-valence RIXS, although the approximation is less justifiable. The theory is implemented in an efficient program that is an extension of the FEFF9 RSGF code, which calculates the spectrum for core-core as well as core-valence RIXS. The RSGF method is advantageous, since relatively large systems can be calculated efficiently, without any restriction on symmetry. In addition, the method is expected to be quite accurate at intermediate photoelectron energies, of the order of 10–100 eV, where other methods may be of limited use due to basis set restrictions and computational cost. The use of the spherical muffin-tin approximation can be problematic at low energies, especially in anisotropic systems.[39] Several illustrative calculations were presented within the quasiparticle approximation where the spectral function is replaced by a δ function, which appears to be a reasonable approximation for these weakly correlated systems. Calculated results for MnO and for anatase TiO_2 based on this quasiparticle approximation are found to agree qualitatively with experimental spectra: the results reproduce both pre-edge and main edge features, the behavior of pre-edge features with varying core-hole interaction strength, and the peak structure due to solid-state effects in valence RIXS. Further investigations including treatments beyond the quasiparticle approximation of Eq. (40) will be reserved for the future. It should be noted that our current formalism for the spectral function is not appropriate for highly correlated materials, although an extension of the quasiboson model Hamiltonian for such cases may be possible.[32,33] Other methods for including strong correlations, such as the Hubbard model, Hubbard plus GW, and T-matrix methods, have been used in calculations of XAS and XPS and could be adapted for calculations of RIXS as well.[45,46] Yet another approach for including strong correlations relevant to this discussion is multiconfigurational multiple-scattering theory.[47] This method has already been used to account for mixing of the core holes in XAS and could be extended to calculations of RIXS. The inclusion of multiple configurations of the valence electrons may also be possible.

ACKNOWLEDGMENTS

We thank T. Ahmed, A. Bansil, R. Markiewicz, E. Shirley, and M. Tromp for useful discussions. This work was supported by DOE BES Grant No. DE-FG03-97ER45623 and was facilitated by the DOE Computational Materials and Chemical Sciences Network (J.J.K. and J.J.R.). J.A.S. gratefully acknowledges the financial support from the Eemil Aaltonen foundation and Magnus Ehrnrooth foundation. The ESRF is acknowledged for providing beam time and technical support (P.G.).

APPENDIX: LOCAL BEHAVIOR OF RIX: DERIVATION OF $T(\Omega)$

The RIXS cross section is given in terms of a product of three Green's functions, that is, $\mathrm{Im}[g^b(E_1)g^c(E2)g^b(E1)^\dagger]$. However, this expression is not very useful, since the spacial arguments of the Green's function must be integrated over all space to obtain the resonance $1/(E1-E2)$. To see this, imagine that we ignore the core-hole potentials in both Green's functions. In this case, we may write the Green's functions in spectal representation, and noting that the wave functions are now orthonormal, we may rewrite the above expression as $|\mathrm{Im}[g(E_2)/(E1-E2+i\Gamma)|^2$, which is what we expect for energies well above threshold, where the effect of the core-hole potential is negligable. While this limit is easy to show analytically, doing so numerically within the real-space MS Green's function formalism proves quite difficult. Below, we derive an alternative expression for the RIXS cross section that takes advantage of the localization of core-hole potential. Let us first define the Hamiltonian operators corresponding to the deep (b) and shallow (c) core holes.

$$h_c = h_0 + V_c, \tag{A1}$$

$$h_b = h_0 + V_b = h_c + \Delta V, \tag{A2}$$

$$\Delta V = V_b - V_c. \tag{A3}$$

We can use these definitions to rewrite the Green's functions as

$$g^b[E_1 - h_b] = \mathbf{1} \Rightarrow g^b = \frac{\mathbf{1} + g^b[h_c + \Delta V]}{E_1}, \tag{A4}$$

$$g^c h_c = -\mathbf{1} + E_2 g^c, \tag{A5}$$

where we have left the energy arguments off of the Green's functions for the sake of brevity. Using these relations gives

$$g^b g^c = \frac{g^c - g^b + g^b \Delta V g^c}{E_1 - E_2} = \frac{D^\dagger g^c - g^b}{E_1 - E_2}, \tag{A6}$$

$$g^c g^{b\dagger} = \frac{g^c - g^{b\dagger} + g^c \Delta V g^{b\dagger}}{E_1^* - E_2} = \frac{g^c D - g^{b\dagger}}{E_1^* - E_2}, \tag{A7}$$

where $D = 1 + \Delta V g^{b\dagger}$. Applying the above relations to $g^b(E_1)g^c(E2)g^b(E1)^\dagger$ gives

$$\begin{aligned} g^b g^c g^{b\dagger} &= \frac{1}{2}[(g^b g^c)g^{b\dagger} + g^b(g^c g^{b\dagger})] \\ &= \frac{1}{2}\left[\frac{(D^\dagger g^c - g^b)g^{b\dagger}}{E_1 - E_2} + \frac{g^b(g^c D - b^{b\dagger})}{E_1^* - E_2}\right] \\ &= \frac{D^\dagger g^c D}{|E_1 - E_2|^2} - \frac{1}{2}\left[\frac{D^\dagger g^{b\dagger}}{|E_1 - E_2|^2} + \frac{g^b g^{b\dagger}}{E_1 - E_2} + \mathrm{h.c.}\right] \end{aligned} \tag{A8}$$

Noting that the second term above is real, we have

$$\mathrm{Im}[g^b g^c g^{b\dagger}] = \frac{D^\dagger \mathrm{Im}[g^c] D}{|E_1 - E_2|^2}. \tag{A9}$$

Finally, we see that the transition matrix element T defined in Sec. II can be related to D, that is,

$$T = DPd. \tag{A10}$$

*Correspondence author: jjr@phys.washington.edu

[1] P. Glatzel, F. M. F. de Groot, and U. Bergmann, Synchrotron Radiat. News **22**, 12 (2009).

[2] F. de Groot and A. Kotani, *Core Level Spectroscopy of Solids* (Taylor and Francis CRC Press, London, 2008).

[3] A. Kotani and S. Shin, Rev. Mod. Phys. **73**, 203 (2001).

[4] W. Schülke, *Electron Dynamics by Inelastic X-Ray Scattering* (Oxford University Press, New York, 2007).

[5] Y. Ma, N. Wassdahl, P. Skytt, J. Guo, J. Nordgren, P. D. Johnson, J.-E. Rubensson, T. Boske, W. Eberhardt, and S. D. Kevan, Phys. Rev. Lett. **69**, 2598 (1992).

[6] Y. Ma, Phys. Rev. B **49**, 5799 (1994).

[7] J. A. Carlisle, E. L. Shirley, E. A. Hudson, L. J. Terminello, T. A. Callcott, J. J. Jia, D. L. Ederer, R. C. C. Perera, and F. J. Himpsel, Phys. Rev. Lett. **74**, 1234 (1995).

[8] S. Shin, A. Agui, M. Watanabe, M. Fujisawa, Y. Tezuka, and T. Ishii, Phys. Rev. B **53**, 15660 (1996).

[9] P. D. Johnson and Y. Ma, Phys. Rev. B **49**, 5024 (1994).

[10] K. Kokko, V. Kulmala, J. A. Leiro, and W. Hergert, Phys. Rev. B **68**, 052503 (2003).

[11] J. Luo, G. T. Trammell, and J. P. Hannon, Phys. Rev. Lett. **71**, 287 (1993).

[12] T. Fujikawa, T. Konishi, and T. Fukamachi, J. Electron Spectrosc. Relat. Phenom. **134**, 195 (2004).

[13] E. L. Shirley, J. A. Soininen, G. P. Zhang, J. A. Carlisle, T. A. Callcott, D. L. Ederer, L. J. Terminello, and R. C. C. Perera, J. Electron Spectrosc. Relat. Phenom. **114-116**, 939 (2001).

[14] J. Jiménez-Mier, J. van Ek, D. L. Ederer, T. A. Callcott, J. J. Jia, J. Carlisle, L. Terminello, A. Asfaw, and R. C. Perera, Phys. Rev. B **59**, 2649 (1999).

[15] P. Glatzel, J. Singh, K. O. Kvashnina, and J. A. van Bokhoven, J. Am. Chem. Soc. **132**, 2555 (2010).

[16] M. van Veenendaal, Phys. Rev. Lett. **96**, 117404 (2006).

[17] A. Kotani, Eur. Phys. J. B **47**, 3 (2005).

[18] L. Campbell, L. Hedin, J. J. Rehr, and W. Bardyszewski, Phys. Rev. B **65**, 064107 (2002).

[19] J. J. Kas, A. P. Sorini, M. P. Prange, L. W. Cambell, J. A. Soininen, and J. J. Rehr, Phys. Rev. B **76**, 195116 (2007).

[20] T. Semba, M. Takahashi, and J.-i. Igarashi, Phys. Rev. B **78**, 155111 (2008).

[21] J. J. Rehr and R. C. Albers, Rev. Mod. Phys. **72**, 621 (2000).

[22] J. J. Rehr, J. J. Kas, F. D. Vila, M. P. Prange, and K. Jorissen, Phys. Chem. Chem. Phys. **12**, 5503 (2010).

[23] K. Jorissen, J. J. Rehr, and J. Verbeeck, Phys. Rev. B **81**, 155108 (2010).

[24] A. L. Ankudinov and J. J. Rehr, Phys. Rev. B **62**, 2437 (2000).

[25] M. P. Prange, J. J. Rehr, G. Rivas, J. J. Kas, and J. W. Lawson, Phys. Rev. B **80**, 155110 (2009).

[26] H. A. Kramers and W. Heisenberg, Z. Phys. **31**, 681 (1925).

[27] A. L. Ankudinov, B. Ravel, J. J. Rehr, and S. D. Conradson, Phys. Rev. B **58**, 7565 (1998).

[28] J. J. Rehr, J. J. Kas, M. P. Prange, A. P. Sorini, Y. Takimoto, and F. Vila, C. R. Phys. **10**, 548 (2009).

[29] T. Åberg, Phys. Scr. **21**, 495 (1980).

[30] J. Tulkki and T. Åberg, J. Phys. B **13**, 3341 (1980).

[31] J. Tulkki and T. Åberg, J. Phys. B **15**, L435 (1982).

[32] L. Hedin, J. Phys. Condens. Matter **11**, R489 (1999).

[33] J. D. Lee, O. Gunnarsson, and L. Hedin, Phys. Rev. B **60**, 8034 (1999).

[34] O. Gunnarsson, V. Meden, and K. Schönhammer, Phys. Rev. B **50**, 10462 (1994).

[35] P. Glatzel, U. Bergmann, J. Yano, H. Visser, J. H. Robblee, W. Gu, F. M. F. de Groot, G. Christou, V. L. Pecoraro, S. P. Cramer *et al.*, J. Am. Chem. Soc. **126**, 9946 (2004).

[36] A. L. Ankudinov, Y. Takimoto, and J. J. Rehr, Phys. Rev. B **71**, 165110 (2005).

[37] J. J. Kas, J. Vinson, N. Trcera, D. Cabaret, E. L. Shirley, and J. J. Rehr, J. Phys. Conf. Ser. **190**, 012009 (2009).

[38] J. A. Bearden and A. F. Burr, Rev. Mod. Phys. **39**, 125 (1967).

[39] D. Cabaret, Y. Joly, H. Renevier, and C. R. Natoli, J. Synchrotron Radiat. **6**, 258 (1999).

[40] P. Glatzel, M. Sikora, and M. Fernández-García, Eur. Phys. J. E Spec. Topics **169**, 207 (2009).

[41] K. Hämäläinen, D. P. Siddons, J. B. Hastings, and L. E. Berman, Phys. Rev. Lett. **67**, 2850 (1991).

[42] H. Hayashi, R. Takeda, Y. Udagawa, T. Nakamura, H. Miyagawa, H. Shoji, S. Nanao, and N. Kawamura, Phys. Rev. B **68**, 045122 (2003).

[43] M. Tromp (private communication).

[44] P. Horsch, W. von der Linden, and W.-D. Lukas, Solid State Commun. **62**, 359 (1987).

[45] H. Jiang, R. I. Gomez-Abal, P. Rinke, and M. Scheffler, Phys. Rev. Lett. **102**, 126403 (2009).

[46] M. Springer, F. Aryasetiawan, and K. Karlsson, Phys. Rev. Lett. **80**, 2389 (1998).

[47] P. Krüger and C. R. Natoli, Phys. Scr. **2005**, 146 (2005).